JOURNAL OF Materials CHEMISTRY

Characterization of organic–inorganic multilayer films by cyclic voltammetry, UV–Vis spectrometry, X-ray photoelectron spectroscopy, small-angle X-ray diffraction and electrochemical impedance spectroscopy

Zhiliang Cheng, Long Cheng, Qiang Gao, Shaojun Dong* and Xiurong Yang*

State Key Laboratory of Electroanalytical Chemistry, Changchun Institute of Applied Chemistry, Chinese Academy of Sciences, Changchun 130022, P. R. China. E-mail: xryang@ns.ciac.jl.cn

Received 2nd January 2002, Accepted 20th March 2002
First published as an Advance Article on the web 18th April 2002

We have employed several techniques, including cyclic voltammetry, UV–Vis spectrometry, small-angle X-ray diffraction, X-ray photoelectron spectroscopy and electrochemical impedance spectroscopy, to characterize the formation processes and interfacial features of ultrathin multilayer films of silicotungstate and a cationic redox polymer on cysteamine-coated Au electrodes self-assembled monolayers. All of these techniques confirm that the multilayer films are built up stepwise as well as uniformly in a layer-by-layer fashion. In particular, the electrochemical impedance spectroscopy is successfully used to monitor the multilayer deposition processes. It has been proved that the electrochemical impedance spectroscopy is a very useful technique in characterization of multilayer films because it provides valuable information about the interfacial impedance features.

1 Introduction

Polyoxometalates (denoted as POMs) are important early transition metal oxygen anion cluster compounds because of the extreme variability, their remarkable molecular tunability, and wide applications in various fields, *e.g.* catalysis, analysis, medicine and material sciences.[1–3] Most of the studies and applications depend on suitable immobilization of these POMs on some substrates. Moreover, POMs with reversible redox activities are an attractive class of modifiers used to modify electrode surfaces. Immobilization of POMs onto electrode surfaces simplifies the studies of POMs and facilitates their applications. Several main modification strategies with a variety of POMs addressed in a recent review include (1) adsorption on electrode surfaces, (2) entrapment into polymer matrixes on electrode surfaces and (3) reductive electrodeposition on electrode surfaces.[4] In addition, there are also some less commonly used modification strategies.[5–8]

Recently, a novel modification strategy of layer-by-layer assembly has been successfully used to modify POMs into multilayered structures on electrode surfaces, based on electrostatic interaction between anionic POMs and cationic compounds or polymers.[9–19] However, much attention has been focused on the preparation of the POMs multilayer films and studies on their electrochemical behavior and electrocatalytic properties. There are only a few reports on the characterization of the formation process of the POMs ultrathin multilayer films.[20,21] It is important to characterize the formation processes and physiochemical features of the multilayer films to understand the properties, mechanism and further applications of the multilayer films. More recently, we described a controlled fabrication of ultrathin multilayer films of silicotungstic heteropolyanion $SiW_{12}O_{40}^{4-}$ on Au electrodes based on cysteamine self assembled monolayers (SAMs).[19] Self-assembly chemisorption is a process by which an oriented monolayer film forms on a surface by the spontaneous adsorption of molecules from solution. It is the most promising strategy for constructing stable, well-defined monolayers on an electrode surface.[22] Here, we choose cysteamine to provide a positively charged surface. In this paper, we provide further characterization of the $SiW_{12}O_{40}^{4-}$ multilayer films by cyclic voltammetry, UV–Vis spectroscopy, small-angle X-ray diffraction, X-ray photoelectron spectroscopy and electrochemical impedance spectroscopy. In addition, micro-Fourier transform infrared spectroscopy and electrochemical quartz crystal microbalance have been used to characterize the POMs multilayer films in our previous report[16] and are not used in this paper. It is worth noting that the electrochemical impedance spectroscopy is successfully used to characterize the interfacial features during formation processes of the multilayer films. The electrochemical impedance spectroscopy is shown to be a very sensitive and useful technique for the characterization of the POMs multilayer films and it is expected to be widely used in the characterization of other multilayer systems.

2 Experimental

2.1 Materials

Cysteamine (denoted as Cyst) of reagent grade was purchased from Sigma. Silicotungstic heteropolyacid $H_4SiW_{12}O_{40}$ (denoted as SiW_{12}) was purchased from Beijing Xinhua Chemical Co. (China). The cationic redox polymer, poly(4-vinylpyridine) partially quaternized with bromoethane and complexed with osmium bis(2,2′-bipyridine) chloride (abbreviated as QPVP-Os) (MW = *ca.* 1.0×10^5), was synthesized and characterized by previously published procedures,[23,24] and was provided by Professor Xi Zhang (Jilin University, China). Structures for these compounds are shown in Fig. 1. All of the other chemicals were of reagent grade and used as received. Solutions were prepared from doubly distilled water that had been purified through an Ultra-pure water system Milli-Q Plus (Millipore Co.). Its resistivity was over 18 MΩ cm. Buffer solutions were prepared from 0.1 M $NaHSO_4$ (pH 1–3.6) and 0.1 M NaAc + HAc (pH 3.6–5.6), with 0.2 M Na_2SO_4 as supporting electrolyte. All solutions were deaerated by bubbling with nitrogen before use.

 DOI: 10.1039/b200035k

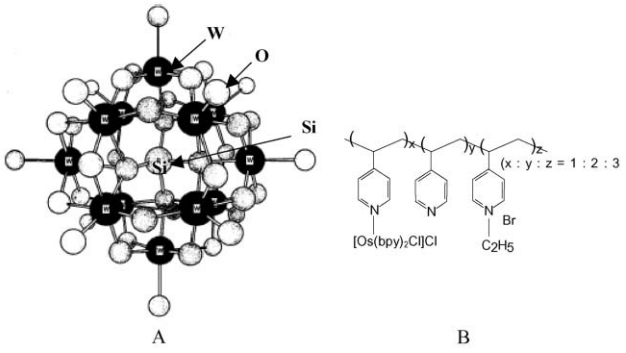

Fig. 1 Chemical formulas of (A) SiW_{12} and (B) QPVP-Os.

2.2 Instrumentation

Cyclic voltammetry experiments were performed with a CHI 600 voltammetric analyzer (CH instruments, USA) in a conventional three-electrode cell. The working electrodes were homemade polycrystalline gold disk electrodes, on which Cyst SAMs, SiW_{12} monolayer and multilayer films were fabricated. The surface of the gold electrode was polished carefully with 1.0, 0.3 and 0.05 μm alumina slurry followed by sonication in distilled water after each polishing step; the surface was then subjected to cyclic potential sweeps between −0.2 and 1.5 V in 1 M H_2SO_4 until a stable CV was obtained (roughness factor of the surface: 1.4). A twisted platinum wire was used as the counter electrode. A Ag/AgCl in saturated KCl solution was used as the reference electrode, against which all potentials were measured and reported. Formal potentials (E_f) of redox couples in CVs were estimated as average values of anodic (E_{pa}) and cathodic (E_{pc}) peak potentials, *i.e.* $E_f = (E_{pa} + E_{pc})/2$; and peak potential separations $\Delta E_p = E_{pa} - E_{pc}$.

UV–Vis absorbance spectrometric experiments were performed using a Shimadzu 3100 UV-VIS-NIR spectrophotometer. Small angle X-ray diffraction (SXRD) was carried out on a Rigaku X-ray diffractometer (D/max γA, using Cu-Kα radiation of wavelength 1.5418 Å). XPS measurements were conducted with an ESCALAB MK spectrometer (VG Co., UK) with a Mg-Kα radiation ($h\gamma$ = 1253.6 eV) as the X-ray source and a pass energy of 50 eV. The SiW_{12}-multilayer films used in the characterization by UV–Vis, SXRD and XPS were deposited on quartz slides using the same method as reported previously.[16] For these measurements, the quartz slide covered with aminopropylsilane was firstly prepared. The multilayer films were fabricated by immersing the quartz substrate in SiW_{12} and QPVP-Os solutions alternately.

Electrochemical impedance spectroscopy measurements were conducted by a Solartron 1250 frequency response analyzer combined with a Solartron 1286 electrochemical interface (Solartron Farnborough, UK). An IEEE-interface (National Instruments, USA) was employed to couple the two Solartron instruments with a PC 586. The impedance spectra were recorded within the frequency range of 0.1–65535 Hz. The amplitude of the applied sine wave potential in each case was 10 mV, while the dc potential was 0.22 V in the presence of $K_4[Fe(CN)_6]$ and $K_3[Fe(CN)_6]$ as redox couple. The same three-electrode configuration as in the above-mentioned cyclic voltammetry experiments was used in the electrochemical impedance spectroscopy measurements.

2.3 Modification procedures

The modification procedures are similar to those in the previous papers[16–19] and are only briefly described here. First, clean Au electrodes were immersed overnight in freshly prepared 10 mM Cyst aqueous solutions to obtain the Cyst self-assembled monolayers (SAMs). Upon protonation, the monolayer provides a positively charged surface. Then the Au electrodes covered with Cyst SAMs (Au/Cyst) were placed in 12 mM SiW_{12} + 0.1 M H_2SO_4 solution and cyclic potential sweeps (CPS) were simultaneously conducted in a potential range between −0.15 and 0.65 V at a scan rate of 0.1 V s^{-1} for 25 cycles. The SiW_{12} monolayer was thus fabricated by the electrochemical growth,[17,18] *i.e.* forming Au/Cyst/SiW_{12}. For fabrication of the SiW_{12} multilayer, its monolayer was placed alternately in QPVP-Os (0.5 mg mL^{-1}in 0.1 M H_2SO_4) and SiW_{12} solutions and the CPS were also simultaneously conducted for 25 cycles in each solution. The SiW_{12} multilayers could be built up in a stepwise fashion using the layer-by-layer deposition. The different thickness of the thus-formed multilayers could be precisely controlled by choosing different steps for the layer-by-layer deposition. For example, Au/Cyst/$n$$SiW_{12}$/$m$QPVP-Os represents a multilayer having $n$$SiW_{12}$ layers and mQPVP-Os layers.

3 Results and discussion

3.1 Cyclic voltammetry:

Because SiW_{12} is an electroactive compound with well-defined reversible redox properties, cyclic voltammetry is a most suitable technique to monitor the deposition processes of the SiW_{12} multilayers and to characterize their electrochemical behavior, by measuring their cyclic voltammograms (CVs) in blank electrolyte solution after depositing each bilayer of QPVP/SiW_{12}. Fig. 2 shows CVs for a series of multilayer chemically modified electrodes (abbreviated as CMEs) of Au/Cyst/$n$$SiW_{12}$/($n$ − 1)QPVP-Os with an increase in number of bilayers from n = 1 to 11, respectively. The multilayers exhibit three couples of redox waves with E_f at *ca.* 0.253, −0.274 and –0.571 V in the potential range from +0.5 to −0.6 V, which corresponds to Os-centered (from QPVP-Os) and W-centered (from SiW_{12}) redox reactions.[16,19] Moreover, the CVs grow gradually and regularly with an increase in the number of bilayers. The multilayer uniformity can be evaluated from the relationship between the number of bilayers and the charge integrated under a certain redox wave, because the charge reflects the amount of the electroactive compound deposited in the multilayer. Taking the second anodic wave as an example, a good linearity of Q_{pa2} *vs.* the number of bilayers has been observed and is shown in the insert of Fig. 2. It is indicated that the multilayers are uniform, with equal amounts of SiW_{12} being deposited at each modification step. The slope of 1.06 μC per SiW_{12} layer corresponds to the adsorption of SiW_{12} with a surface coverage of *ca.* 1.1 × 10^{-10} mol cm^{-2} if the geometric area of the gold electrode (0.05 cm^2) is employed,

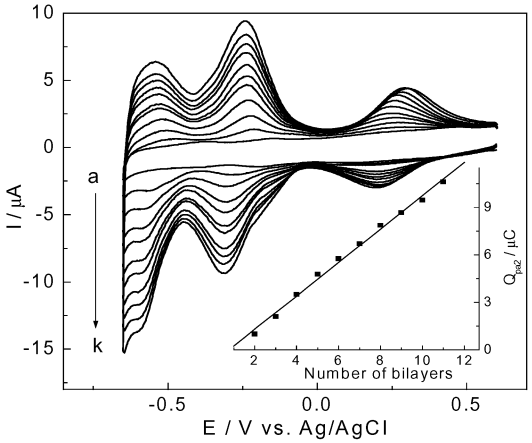

Fig. 2 CVs of multilayer CMEs of Au/Cyst/nSiW_{12}/(n − 1)QPVP-Os in pH 4.6 buffer solution with an increase in the number of bilayers from n = 1 to 11 (shown from curves a to k) respectively. Scan rate: 0.1 V s^{-1}. The insert shows a relationship between the number of bilayers and the charge of the second anodic peak.

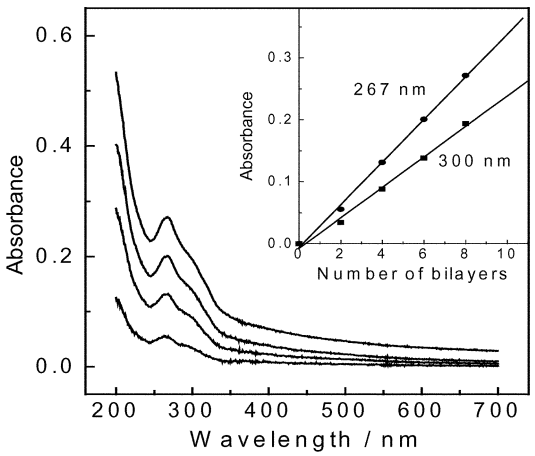

Fig. 3 UV–Vis spectra of multilayer films of nSiW$_{12}$/nQPVP-Os deposited on a quartz slide with increase in number of bilayers from $n = 2$, 4, 6 to 8 shown from lower to upper curves, respectively. The insert shows the relationships between the number of bilayers and the absorbance at 267 and 300 nm.

which suggests addition of approximately one monolayer of SiW$_{12}$ at each modification step.

3.2 UV–Vis spectrometry

UV–Vis spectrometry is also a very useful technique to follow the deposition process of multilayer films containing chromophores.[14–16,21,25,26] Fig. 3 shows UV–Vis spectra of multilayer films of nSiW$_{12}$/nQPVP-Os with an increase in number of bilayers from $n = 2$, 4, 6 to 8, respectively. There are two main absorption peaks at *ca.* 267 and 300 nm. The absorption peak at 267 nm is characteristic of the oxygen–tungsten charge-transfer band of SiW$_{12}$.[1,27] The other band at 300 nm can be assigned to π–π* transition of the bipyridine groups of QPVP-Os.[28] As shown in the insert of Fig. 3, the absorption values at 267 and 300 nm increase linearly with the number of bilayers, which proves that each deposition adds the same amount of modifier onto the resulting multilayer films. It also indicates that the stepwise deposition of the multilayer films is very uniform and regular. Moreover, both of the two lines passing through the origin reflect the equal amount of SiW$_{12}$ deposited onto the precursor layer and the subsequent QPVP-Os layers. The results of the UV–Vis spectrometry measurements are consistent with those of the cyclic voltammetry.

3.3 Small-angle X-ray diffraction

Thickness and homogeneity of the QPVP-Os and SiW$_{12}$ multilayer films have been measured by small-angle X-ray diffraction (SAXD). Taking a multilayer film consisting of 8 bilayers of SiW$_{12}$/QPVP-Os as an example, its SAXD spectrum is given in Fig. 4. A series of Kiessig fringes appear with 2 theta at 1.08°, 1.46° and 1.81°, respectively. The Kiessig fringes arise from the interference of the X-ray beams reflected at the substrate–film and film–air interfaces.[29,30] The presence of Kiessig fringes is characteristic of an uniform and homogenous multilayer film. However, there is no Bragg peak observed in the SAXD spectrum. Bragg peaks are characteristic of ordered lattices and observable only when the film has regions of sufficiently different electron density.[21,31] Therefore, the absence of any Bragg peaks may result from the electron density of the two consecutive layers not being large enough to yield a sufficient contrast.[21] In addition, the absence of Bragg peaks may also indicate an interpenetrated structure between neighboring layers. Similar phenomena were found for other multilayer systems based on the electrostatic interaction between polycations and polyanions.[31–33] The thickness of the multilayer film was estimated from the oscillation period.[34]

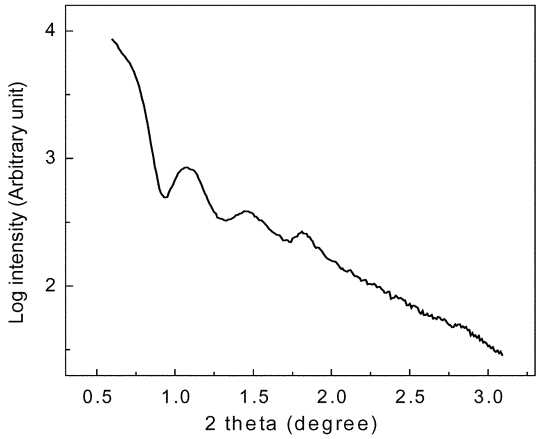

Fig. 4 Small-angle X-ray diffraction (SAXD) of a multilayer film of 8SiW$_{12}$/8QPVP-Os deposited on a quartz slide.

The total thickness of the multilayer film consisted of 8 bilayers of SiW$_{12}$/QPVP-Os and was calculated to be 243.7 Å. Therefore, the average thickness for a bilayer of SiW$_{12}$/QPVP-Os is *ca.* 30.5 Å, which is reasonable when considering the diameter of SiW$_{12}$ being *ca.* 12 Å and the multilayer deposition conducted in salt-containing solutions that will result in much thicker film.[28]

3.4 X-Ray photoelectron spectroscopy

X-Ray photoelectron spectroscopy (XPS) measurements were conducted to confirm the presence of silicon (Si), tungsten (W), and osmium (Os) elements in the multilayer films. Recorded were a survey scan in a binding energy window between 0 and 1250 eV as well as several high-resolution XPS spectra for C 1s, O 1s, N 1s, Si 2p, W 4f and Os 4f levels. The C 1s XPS peak is located at 284.6 eV, which was referred to charging calibration. The O 1s and N 1s appear at 530.8 and 398.5 eV, respectively. The wide peak shapes of the O 1s and N 1s XPS signals are indicative of more than one component responsible for the two XPS peaks. It was found in our previous report that there are at least two origins for the O 1s XPS signal (from POMs and chemisorbed water) and also for the N 1s XPS signal (from quaternized pyridine group of QPVP and 2,2′-bipyridine of Os(bpy)$_2$Cl$_2$).[16] The survey scan and the XPS spectra for C 1s, O 1s and N 1s levels are not discussed in detail due to their complex origins and less characteristic features for the two modifiers of SiW$_{12}$ and QPVP-Os. In contrast, the XPS spectra for Si 2p, W 4f and Os 4f levels are depicted in Fig. 5 to show that the multilayer films contain the Si, W and Os elements. Undoubtedly, the Si 2p and W 4f XPS signals have the only origin of SiW$_{12}$, while the Os 4f XPS signal must result from QPVP-Os. In the binding energy window between 98.5 and 109.5 eV, a well-resolved Si 2p XPS signal appears at *ca.* 102.6 eV. In addition, the W 4f XPS signal is always present in doublet shape with binding energy located at 35.5 and 37.5 eV for W 4f$_{7/2}$ and 4f$_{5/2}$ levels, which are closely similar to the reported data of 35.5 and 37.4 eV for the K$_4$SiW$_{12}$O$_{40}$ powder.[35] These binding energy values are consistent with the spin orbit splitting of the W 4f level in oxidation state of +6, as expected for SiW$_{12}$O$_{40}^{4-}$. In the binding energy window of 42.5 to 62.5 eV, a high-resolution doublet XPS signal from Os center appears at 50.5 and 52.9 eV, corresponding to Os 4f$_{7/2}$ and 4f$_{5/2}$ levels. The binding energy values for Os 4f$_{7/2}$ and 4f$_{5/2}$ levels found here are in good agreement with our previous results of 50.5 and 53.0 eV for other multilayer films comprised of SiMo$_{11}$V and QPVP-Os.[16] Therefore, the XPS results prove that the multilayer films are composed of SiW$_{12}$ and QPVP-Os.

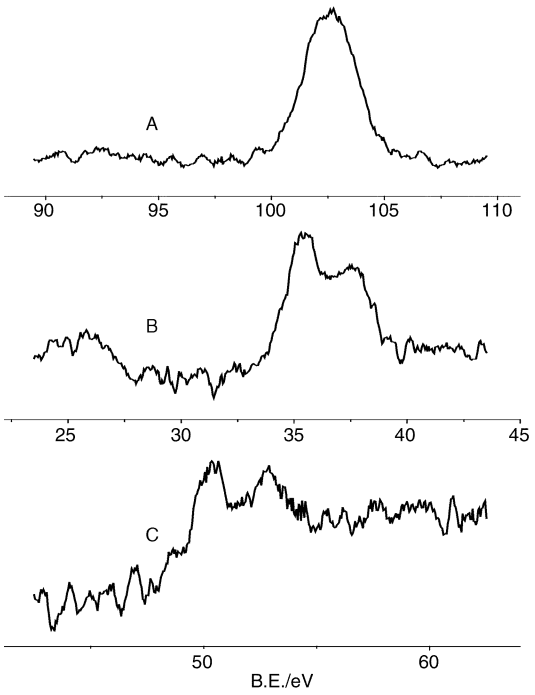

Fig. 5 XPS spectra of a multilayer film of $8SiW_{12}$/8QPVP-Os deposited on a quartz slide for (A) Si 2p, (B) W 4f and (C) Os 4f.

3.5 Electrochemical impedance spectroscopy

Electrochemical impedance spectroscopy is an effective method to investigate the interfacial properties of modified electrodes.[36–40] Modification of the conductive supports may alter some features of the impedance data on the electrode surfaces, *e.g.* the double-layer capacitance and charge-transfer resistance, *etc.* Impedance methods are also attractive because of the small sinusoidal potentials that are used, as opposed to the wide potential window used in CV. Here we demonstrate that the electrochemical impedance spectroscopy is a unique technique in monitoring the deposition processes of multilayer formation and in characterizing the interfacial properties of the multilayer films.

The complex impedance can be presented as a sum of real, Z_{re}, and imaginary, Z_{im} components that are mainly contributed by the resistance and capacitance of the cell. Fig. 6

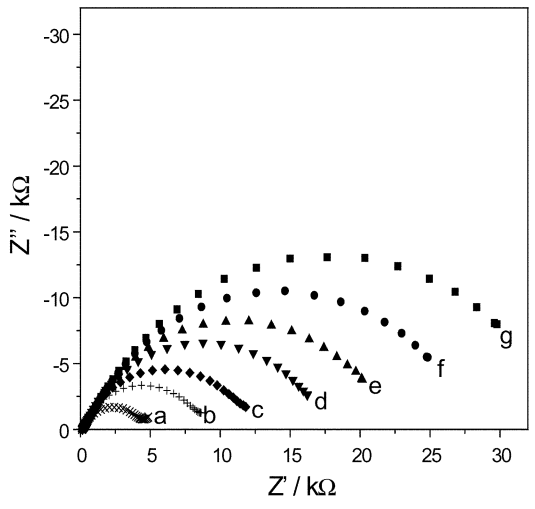

Fig. 6 Complex plane impedance plots of multilayer CMEs of Au/Cyst/nSiW$_{12}$/(n − 1)QPVP-Os with increase in number of bilayers from n = 3 to 9 (shown from curves a to g) respectively. Electrolyte solution: 0.1 M KCl containing 5 mM each of $K_4[Fe(CN)_6]$ and $K_3[Fe(CN)_6]$. The frequency range is between 0.1 Hz and 65535 Hz with a signal amplitude of 10 mV. DC potential: 220 mV.

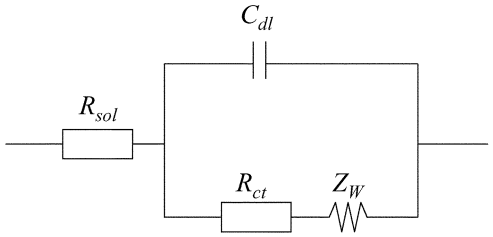

Fig. 7 General equivalent circuit for the electrochemical impedance spectroscopy measurements performed at the Au electrodes modified with multilayer films in the presence of $[Fe(CN)_6]^{3-/4-}$ as a redox probe.

shows typical impedance features for multilayer electrodes with various layer numbers in aqueous solution containing the redox probe of $Fe(CN)_6^{4-/3-}$. It is reasonable to believe that only reaction of $Fe(CN)_6^{4-}/^{3-}$ has occurred at the Au–film interface at the formal potential of redox couples. Significant changes in the impedance spectra are observed during stepwise formation of the multilayer films on the electrode. First, the line part at the low frequencies appears only at the early formation stage of the multilayer films with low bilayer numbers (*e.g.* $n = 3$ as shown by curve a in Fig. 6), but it is absent for multilayer films with higher bilayer numbers (*e.g.* $n > 4$ as shown by curves from c to g in Fig. 6). Secondly, it was clearly observed that diameters of the semicircle parts increase with the film growth, which means that the reaction is under kinetic control at any frequency in the range studied. Finally, the low-frequency linear-mass-transfer region is hardly observed because the reaction is under kinetic control over the entire frequency range.

In the presence of redox probe in solution, Randles' equivalent circuit is well-established to fit the impedance responses of the electrode–solution interface, which was successfully used to fit the system of multilayer films.[41] The circuit is illustrated in Fig. 7. The total impedance is determined by several parameters: (1) the double-layer capacitance, C_{dl}, of the diffuse Gouy–Chapman at the membrane electrode–solution interface; (2) charge transfer resistance R_{ct}; (3) Warburg element Z_w; (4) electrolyte resistance R_{sol}. Maybe this equivalent circuit used for the calculation is still too simple and more components should be introduced. However, considering the aim of this work, we prefer to avoid a more complicated circuit.

A convenient procedure of data evaluation is to represent the data in terms of Bode plots. Fig. 8 shows one of the responses

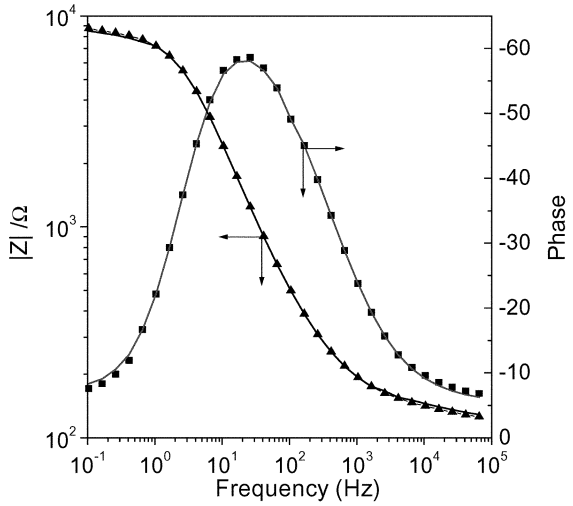

Fig. 8 Bode representation for Au/Cyst/$5SiW_{12}$/4QPVP-Os of (■) phase angle α and (▲) impedance modulus $|Z|$ as a function of applied frequency. The solid line (—) represents their fitted curves.

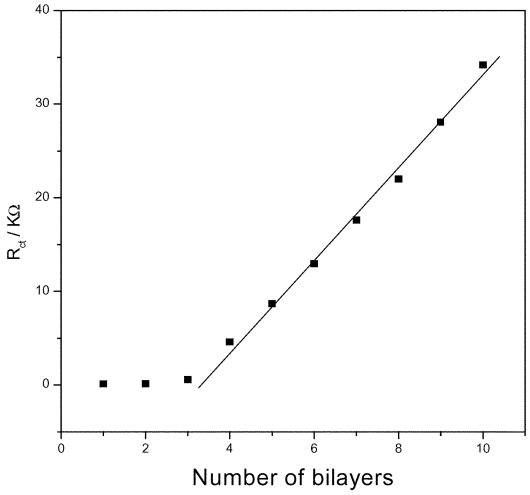

Fig. 9 The relationship between R_{ct} *vs.* the number of bilayers. The data were obtained from Fig. 6.

and its fitted dispersion data. The fitted results fit well with the experimental data, demonstrating that the equivalent circuit of Fig. 7 is a suitable model for the systems studied here.

Some impedance parameters (R_{ct}, C_{dl}) were chosen in order to show the nature of the film. The circuit element of most interest to this work is R_{ct} because it often relates directly to the accessibility of the modified gold electrode and reflects the flow of charge across the modified interface into the electrode.

Fig. 9 shows the R_{ct} change with stepwise deposition of SiW_{12} and QPVP-Os layers. The value of R_{ct} in the initial bilayer is smaller compared with the outer bilayers. The curve shows a good linear relationship between R_{ct} and bilayer numbers from the fourth bilayer, but the initial R_{ct} values ($n < 4$) were irregular compared with the subsequent ones.

The following mechanisms for electron transfer between redox couples and the modified electrode can be envisaged: (1) the electroactive species could permeate through the film and react at the electrode surface; (2) the electroactive species could directly diffuse to bare spots on the electrode through pores or defects of the film.

The nonlinear increase of R_{ct} with the number of bilayer suggests a different structure in the initial bilayer than in the rest of the film. In the initial film, the probe can access the surface of the electrode through defects and pinholes in the film. When the film grows thicker, pathways to the electrode surface will become fewer and longer.

The initial bilayer numbers with R_{ct} are not linear. This phenomenon is consistent with the results reported by Lvov and Sackmann.[42,43] It is not surprising that the composition of the initial bilayers could differ from that in the subsequent bilayers, where the same electrostatic factors control the composition of each succeeding layer. It may be due to the fact that the multilayer films are less compact for initial bilayer numbers, and that it is possible to contain water or ions from the electrolyte in the porosity of the film. As the film grows, it becomes progressively compact.

4 Conclusions

Ultrathin multilayer films were deposited based on electrostatic interaction between anionic silicotungstate SiW_{12} and cationic redox polymer QPVP-Os on Au electrodes pre-coated cysteamine SAMs. Cyclic voltammetry, UV-vis spectrometry, small-angle X-ray diffraction, X-ray photoelectron spectroscopy and electrochemical impedance spectroscopy were employed to characterize the formation processes and interfacial features of the resulting multilayer films. Cyclic voltammetry and UV-vis spectrometry prove the linear dependence of the amount of deposited modifiers on the bilayer number of the resulting multilayers. XPS measurements demonstrate the composition of the multilayers being SiW_{12} and QPVP-Os. The small-angle X-ray diffraction measurements determined the average thickness for a bilayer of SiW_{12}/QPVP-Os to be *ca.* 30.5 Å. In particular the electrochemical impedance spectroscopy was successfully used to monitor the multilayer deposition processes. We found that the semicircle diameter grows larger regularly with the stepwise formation of the multilayer films. Moreover, the charge-transfer resistance R_{ct} increases linearly with the bilayer numbers. It is suggested that (1) the multilayer films are deposited on the substrate electrode in a very uniform and regular way and (2) the redox reaction of the redox couple of $Fe(CN)_6^{4-/3-}$ is impeded gradually by the multilayer films. Our experimental results prove that the electrochemical impedance spectroscopy is a very useful technique in characterization of multilayer films because it provides valuable information about the interfacial impedance features. Therefore, it is reasonable to expect that electrochemical impedance spectroscopy will be widely used in other multilayer systems. All of these techniques give the consistent result that the multilayer films were fabricated stepwisely as well as uniformly in a layer-by-layer fashion. In addition, these novel multilayer films may find potential applications in electrochromism, photoelectrochemistry, sensors, catalysis, light imaging, and other thin-film molecular devices because the thickness, composition, and physicochemical properties of the multilayers can be varied, controlled, and tailored to meet the practical needs at a molecular level.

Acknowledgement

This work was supported by the National Natural Science Foundation of China.

References

1 M. T. Pope, *Heteropoly and isopoly oxometalates*, Springer-Verlag, New York, 1983, p. 321.
2 M. T. Pope and A. Muler, *Angew. Chem., Int. Ed. Engl.*, 1991, **30**, 34.
3 C. L. Hill, (guest editor) *Chem. Rev.*, 1998, **98**. The whole volume is dedicated to polyoxometalates.
4 M. Sadakane and E. Steckhan, *Chem. Rev.*, 1998, **98**, 219.
5 B. Keita, N. Dellero and L. Nadjo, *J. Electroanal. Chem.*, 1991, **302**, 47.
6 A. M. Bond, J. B. Cooper, F. Marken and D. M. Way, *J. Electroanal. Chem.*, 1995, **396**, 407.
7 A. Papadakis, A. Souliotis and E. Papacconstantinou, *J. Electroanal. Chem.*, 1997, **435**, 17.
8 W. Song and C. Sun, *Chin. Chem. Lett.*, 1999, **9**, 1109.
9 D. Ingersoll, P. J. Kulesza and L. R. Faulkner, *J. Electrochem. Soc.*, 1994, **141**, 140.
10 A. Kuhn and F. C. Anson, *Langmuir*, 1996, **12**, 5481.
11 A. Kuhn, N. Mano and C. Vidal, *J. Electroanal. Chem.*, 1999, **462**, 187.
12 G. M. Kloster and F. C. Anson, *Electrochim. Acta*, 1999, **44**, 2271.
13 C. Sun, J. Zhao, H. Xu, Y. Sun, X. Zhang and J. Shen, *J. Electroanal. Chem.*, 1997, **435**, 63.
14 C. Sun and J. Zhang, *Electroanalysis*, 1997, **9**, 1365.
15 C. Sun and J. Zhang, *Electrochim. Acta*, 1998, **43**, 943.
16 L. Cheng, L. Niu, J. Gong and S. Dong, *Chem. Mater.*, 1999, **11**, 1465.
17 L. Cheng and S. Dong, *Electrochem. Commun.*, 1999, **1**, 159.
18 L. Cheng and S. Dong, *J. Electrochem. Chem.*, 2000, **481**, 168.
19 L. Cheng and S. Dong, *J. Electrochem. Soc.*, 2000, **147**, 606.
20 I. Ichinose, H. Tagawa, S. Mizuki, Y. Lvov and T. Kunitake, *Langmuir*, 1998, **14**, 187.
21 F. Caruso, D. G. Kurth, D. Volkmer, M. J. Koop and A. Muller, *Langmuir*, 1998, **14**, 3462.
22 H. Shen, J. E. Mark, C. J. Seliskar, H. B. Mark, Jr. and W. R. Heineman, *J. Solid State Electrochem.*, 1997, **1**, 148–154.
23 A. Aoki, R. Rajagoppalan and A. Heller, *J. Phys. Chem.*, 1995, **99**, 5102.

24 A. P. Doherty, R. J. Forster, M. R. Smyth and J. G. Vos, *Anal. Chim. Acta*, 1991, **255**, 45.
25 M. Ferreira and M. F. Rubner, *Macromolecules*, 1995, **28**, 7170.
26 X. Zhang, M. Gao, X. Kong, Y. Sun and J. Shen, *J. Chem. Soc., Chem. Commun.*, 1994, **11**, 1055.
27 W. Wang, X. H. Zhu and J. F. Liu, *Yingyong Huaxue*, 1993, **10**, 88.
28 J. Q. Sun, Y. P. Sun, S. Zou, X. Zhang, C. Q. Sun, Y. Wang and J. C. Shen, *Macromol. Chem. Phys.*, 1999, **200**, 840.
29 G. Decher and J. Schmitt, *Prog. Colloid Polym. Sci.*, 1992, **89**, 160.
30 Y. Lvov and G. Decher, *Langmuir*, 1993, **9**, 481.
31 J. Schmitt, G. Decher, W. J. Dressick, S. L. Brandow, R. E. Geer, R. Shashidhar and J. M. Calvert, *Adv. Mater.*, 1997, **9**, 61.
32 G. Decher, *Science*, 1997, **277**, 1232.
33 M. Lutt, M. B. Fitzsimmons and D. Q. Li, *J. Phys. Chem. B*, 1998, **102**, 400.
34 P. Tippmann-krayer, H. Mohwald and Yu. Lvov, *Langmuir*, 1991, **7**, 2298.
35 J. Wang, Z. Wu, H. Zhang, Z. Zhao, X. Wang and Q. Wei, *Chem. J. Chin. Univ.*, 1992, **13**, 1428.
36 H. O. Finklea, D. A. Snider, J. Fedyk, E. Sabatani, Y. Gafni and I. Rubinstein, *Langmuir*, 1993, **9**, 3660.
37 H. Taira, K. Nakano, M. Maeda and M. Takagi, *Anal. Sci.*, 1993, **9**, 199.
38 A. Bardea, F. Patolsky, A. Dagan and I. Willner, *Chem. Commun.*, 1999, **21**, 21.
39 F. Patolsky, M. Zayats, E. Katz and I. Willner, *Anal. Chem.*, 1999, **71**, 3171.
40 F. Patolsky, E. Katz, A. Bardea and I. Willner, *Langmuir*, 1999, **15**, 3703.
41 J. J. Harris and M. L. Bruening, *Langmuir*, 2000, **16**, 2006.
42 M. Stelzle and E. Sackmann, *Biochim. Biophys. Acta*, 1989, **981**, 135.
43 Y. Lvov, K. Ariga, I. Ichinose and T. Kunitake, *J. Am. Chem. Soc.*, 1995, **117**, 6117.